Hindawi
Journal of Applied Mathematics
Volume 2023, Article ID 1146872, 13 pages
https://doi.org/10.1155/2023/1146872

Research Article

Interaction of Two Rigid Spheres Oscillating in an Infinite Liquid under the Control of a Magnetic Field

Shreen El-Sapa [1] and Wedad Albalawi [2]

[1] *Department of Mathematics, Faculty of Science, Damanhour University, Damanhour 22511, Egypt*
[2] *Department of Mathematical Sciences, College of Sciences, Princess Nourah bint Abdulrahman University, P.O. Box 84428, Riyadh 11671, Saudi Arabia*

Correspondence should be addressed to Shreen El-Sapa; s_elsapa82@sci.dmu.edu.eg

Received 10 February 2023; Revised 28 February 2023; Accepted 25 April 2023; Published 5 May 2023

Academic Editor: Oluwole D. Makinde

The transient creeping motion of two rigid spheres oscillating in a boundless viscous fluid beneath the impact of the magnetic field is investigated. There is no slippage associated with a Stokes flow on the two rigid spherical surfaces with different sizes and radii. The solutions can be obtained using the boundary collocation scheme at low Reynolds numbers. The unsteady real and imaginary drag coefficients are estimated on the hard spherical particles. These coefficients are computed in tables for various parameters and illustrated graphically. The frequency parameter and Hartmann number also play a significant role in this study where the drag coefficients decrease or increase by 100 percent after the value of $\kappa = 5.0$. Using available literature data, we tested the accuracy and reliability of our results.

1. Introduction

There has been a lot of research into how the dynamics of fluid techniques interact with oscillating particles. As a result of these studies, wave packs experienced by offshore forms can be estimated and ocean vehicle motion can be predicted from a functional view. The relations between two rigid spheres oscillating in a viscid flow along their linking axis of symmetry are introduced in [1]. By using direct numerical simulations [2], the periodic couplings of two hard spheres that move uniformly side by side in a fluid stream are studied. On the other hand, an investigation of hard spheres swimming into an oscillating fluid flow is investigated in [3]. Therefore, [4] introduces interactions around oscillating particles in a steady streaming flow. Further, the study of the impact of adjoining boundaries upon rotationally oscillating spheres in viscous fluids is presented experimentally and theoretically in [5]. In a pendulous flow, two solid spheres immersed in a viscid fluid move perpendicularly to the direction of the flow, and a little separation distance between them is presented by [6]. Therefore, Faltas and El-Sapa [7] proposed a solution to the problem of a couple of spherical objects swimming in a viscid liquid at a low Reynolds number by employing the collocation technique.

In cancer therapy, magnetohydrodynamics (MHD) plays a significant role in magnetic drug targeting. There is a model demonstrating a setup for examining the effects of an external magnetic field containing a magnetic carrier substance that interacts with blood flow. In medication, MHD liquid streams and fluctuations in different mathematical shapes applicable to human body parts are fascinating and essential exploration regions. Plumpton and Ferraro [8] researched the influence of the homogenous magnetic field upon the torsional fluctuations of a perpetual sphere. Also, Stewartson [9] introduced symmetrically oscillating objects at the infinite conductivity limit. In 1965, [10] investigated the impacts of incompressible magnetic fields, Coriolis powers, and their communication on physical drag. In 2015,

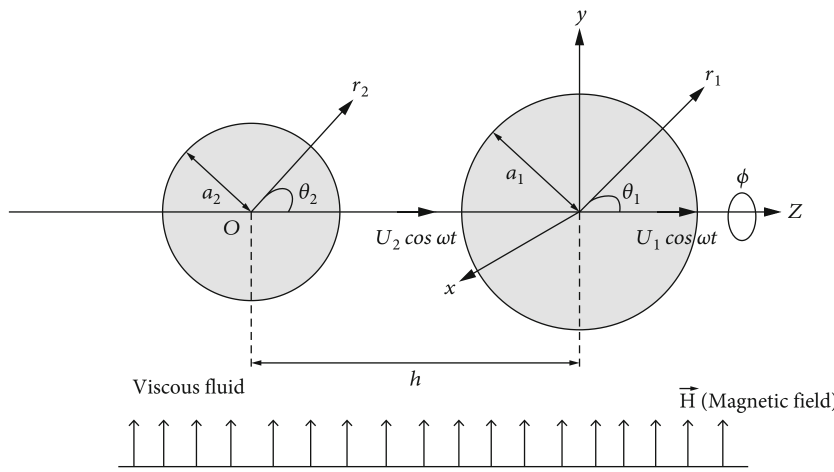

Figure 1: Magnetic field-induced rectilinear fluctuations of two hard spheres in viscid liquid.

Barakat [11] presented an issue of the MHD soundness of an oscillating liquid within sight of a longitudinal magnetic field. This work settled utilizing a PC calculation that decided the steady and unsteady zones under the changed values of the acting magnetic field. Besides, Wentzell [12] correspondingly contemplated the torsional motions of a profoundly directing low viscosity of a drop enclosed in a uniform magnetic field. Under the impact of the magnetic field, there are many applications of MHD such as the solitary waves propagation, and stability conditions of the cold plasma are analyzed using the reductive perturbation method by Adel et al. [13, 14] and also in nuclear reactors and nanofluids in [15, 16].

Furthermore, the numerical explanations of the equations coupled between magnetic and velocity fields for a completely created MHD move via an unplugged direct channel of the rectangular area. Hence, Cai et al. [17] assumed the combination strategy collocation with a plan of a storm under the impact of a magnetic field. A careful examination of MHD applications and mathematical demonstrations in organic frameworks was directed by Rashidi et al. [18]. Also, Dhivya et al. [19] used a Wrench Nicholson plot and limited contrast plans for solving an issue of a characteristic convective progression of an isochoric and synthetically responsive viscid liquid about an oscillating vertical chamber encased in a permeable structure. A computational strategy for a thick incompressible magnetohydrodynamic stream in a pivoting channel under magnetic field impacts was also determined by Li et al. [20]. The semianalytical method for the study of the translational movement of two rigid spheres is considered by El-Sapa [21] and El-Sapa and Faltas [22] to compute the mobility coefficients and set the circumstances on the spheres' surfaces mathematically utilizing the limit collocation technique. A semianalytical model for analyzing rectilinear fluctuations of a solid particle engaged in an incompressible micropolar fluid specified by a rigid plane wall has been developed by Yadav et al. [23]. In a plane wall, the particle oscillates rectilinearly. Moreover, recently, El-Sapa and Alhejaili [24] explored the influence of slippage length on the movement of two inflexible spheres oscillating via a Stokes flow about their axis of symmetry through the line linking their poles and the global solutions constructed upon the superposition of the actual solutions in the two spherical coordinate techniques by a collocation procedure.

This work focuses on oscillating two rigid spheres moving inside a viscid liquid along the line joining their centers at different velocities affected by a magnetic field. Semianalytical solutions for the velocity fields are introduced. In addition, the hydrodynamic drag force coefficients of the real and the imaginary parts for different frequencies, detachment space, size ratio, Hartmann number, and speed proportions are obtained and discussed. In general, the forces decrease or increase gradually at the value of $\kappa = 5.0$. For instance, the steady state with pure oscillations and no-slip express is confirmed as convergent and accurate.

2. Magneto-Stokes Field Equations

Low Reynolds number assumptions are covered by the general equations of the incompressible magnetoviscid liquid [17, 22]:

$$\nabla . \vec{q} = 0, \tag{1}$$

$$\frac{\partial \vec{q}}{\partial t} = -\frac{1}{\rho} \nabla p + \nu \nabla^2 \vec{q} + \frac{1}{\rho} \vec{F}^E, \tag{2}$$

considering the velocity $\vec{q}$, density ρ, fluid pressure p, kinematic viscosity of the fluid $\nu (= \mu/\rho)$, and dynamic viscosity μ. Therefore, $\vec{F}^E$ is the outward magnetoforce given as

$$\vec{F}^E = -c^{-1} \vec{B} \wedge \vec{J} = -c^{-2} \sigma \vec{B} \wedge \left(\vec{q} \wedge \vec{B} \right). \tag{3}$$

Consequently, c is the light speed, $\vec{B}$ is the vector of the induced magnet, $\vec{J}$ is the influx of density, μ_0 is the penetrability magnet, and $\vec{H}$ is the field vector of the magnet. Hence, by utilizing Lorentz's power created by

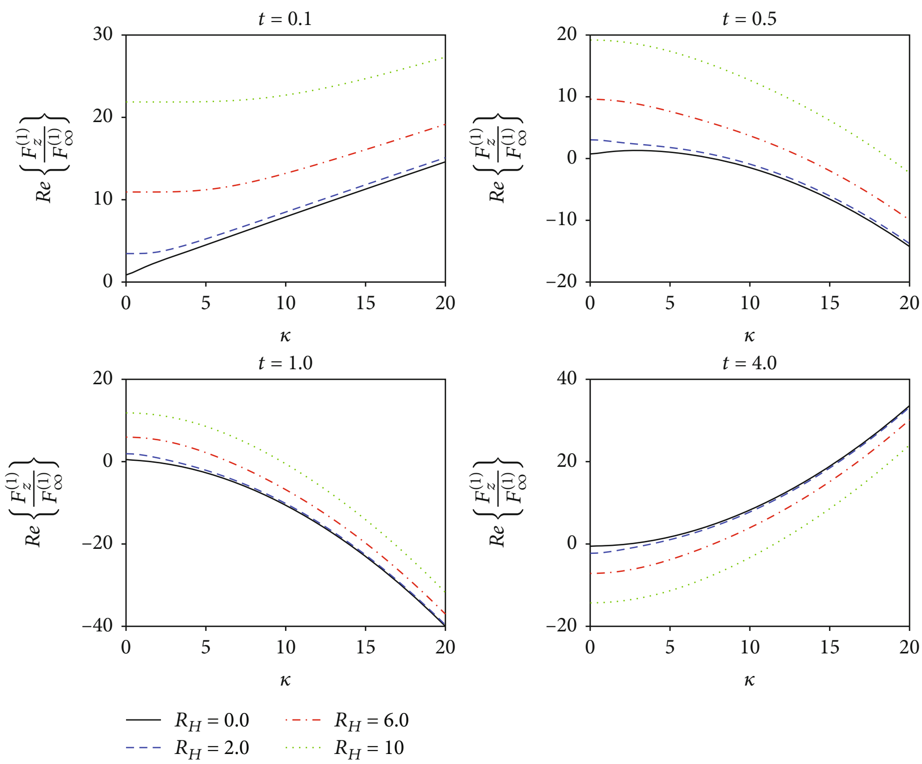

Figure 2: Time-dependent distribution of real friction force on a sphere a_1 versus the frequency for different Hartmann numbers with $h/a_1 + a_2 = 1.5$, $a_2/a_1 = 1.0$, and $U_2/U_1 = 1.0$.

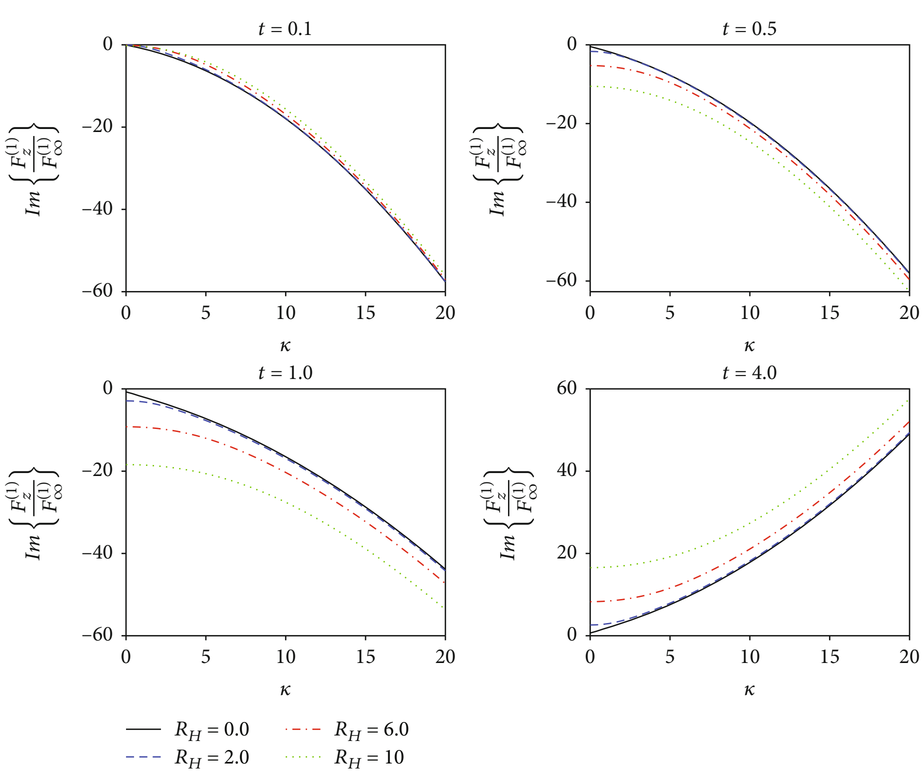

Figure 3: Time-dependent distribution of imaginary friction force on a sphere a_1 versus the frequency for different Hartmann numbers with $h/a_1 + a_2 = 1.5$, $a_2/a_1 = 1.0$, and $U_2/U_1 = 1.0$.

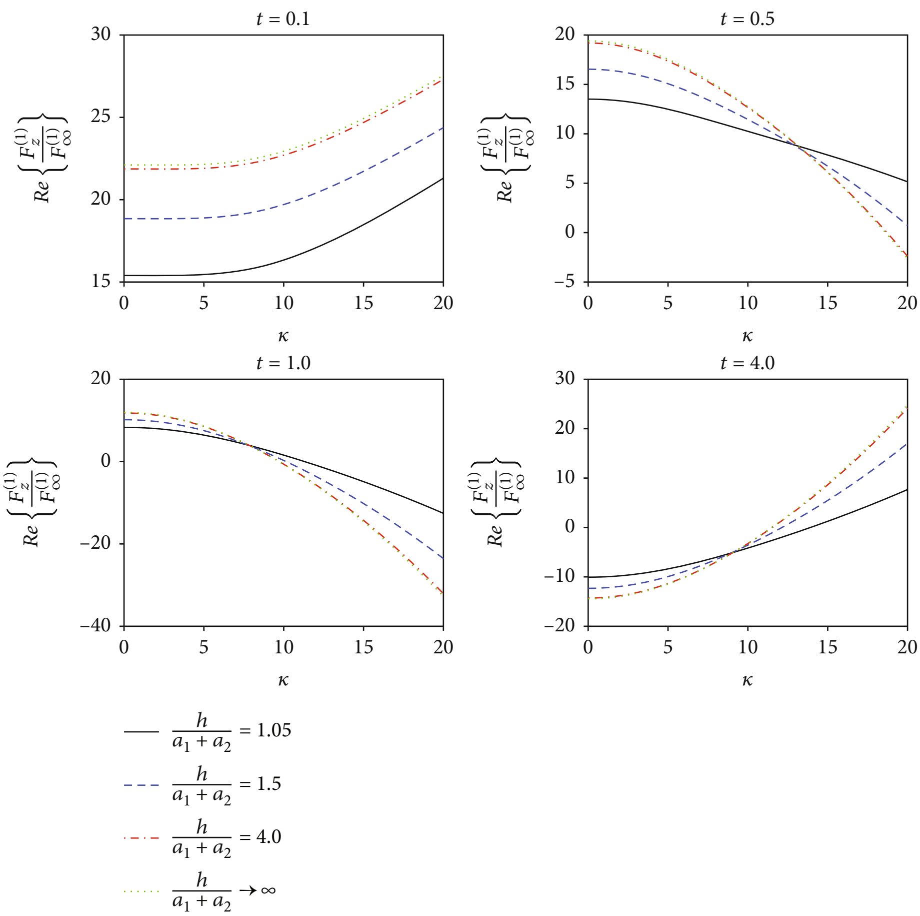

Figure 4: Time-dependent distribution of real friction force on a sphere a_1 versus the frequency for different separation parameters with $a_2/a_1 = 4.0$, $U_2/U_1 = 1.0$, and $R_H = 10.0$.

[23] where the vector of magnetization is disregarded except if the magnetic field is the areas of extreme strength, speed of the liquid is not normal to the vector of magnetic induction that maintains the stream axisymmetric and creeping movements, so

$$\left\langle \left(\vec{q} \wedge \vec{B} \right) \wedge \vec{B} \right\rangle = -\frac{1}{2} B_0^2 \vec{q}, \tag{4}$$

where B_0 is a constant. Besides, we have equation (3) that pursues

$$\vec{F}^E = \frac{-\sigma B_0^2}{c^2} \vec{q} = \frac{-B_0^2}{\eta \mu_0} \vec{q} = -\mu a^{-2} R_H^2 \vec{q}, \tag{5}$$

where $\eta = c^2/\sigma\mu_0$ is the parameter of diffusivity, σ is the electroconductivity, and R_H is the number of Hartmann.

3. The Mathematical Formulation

Further, it is assumed that the unbending molecule of radius a oscillates axisymmetrically under the circumstances $\vec{q}/U = \cos \omega t \vec{e}_z$ as $r \longrightarrow \infty$ on the limit and impedes in an infinite viscid liquid under the normal magnetic field. Thus, $\vec{e}_z$ is the vector units parallel to the axis z, U is typically the speed, and ω is the hesitancy oscillations. Moreover, we suppose $(\vec{e}_r, \vec{e}_\theta, \vec{e}_\phi)$ is the corresponding vector units and (r, θ, ϕ) is a spherical polar coordinates.

3.1. The Applied Periodical Functions. The following are functions in terms of the time dependency of stream function ψ:

$$\begin{Bmatrix} \Psi(r,\theta;t) \\ P(r,\theta;t) \\ \vec{q}(r,\theta;t) \end{Bmatrix} = \mathrm{Re} \begin{Bmatrix} \psi(r,\theta)e^{-i\omega t} \\ p(r,\theta)e^{-i\omega t} \\ \vec{q}(r,\theta)e^{-i\omega t} \end{Bmatrix}. \tag{6}$$

The two-dimensional velocity vector is

$$\vec{q}(r,\theta) = \langle q_r(r,\theta), q_\theta(r,\theta) \rangle. \tag{7}$$

3.2. The Dimensionless Quantities. By using U for the scale of velocity, the particle, and a for the length in

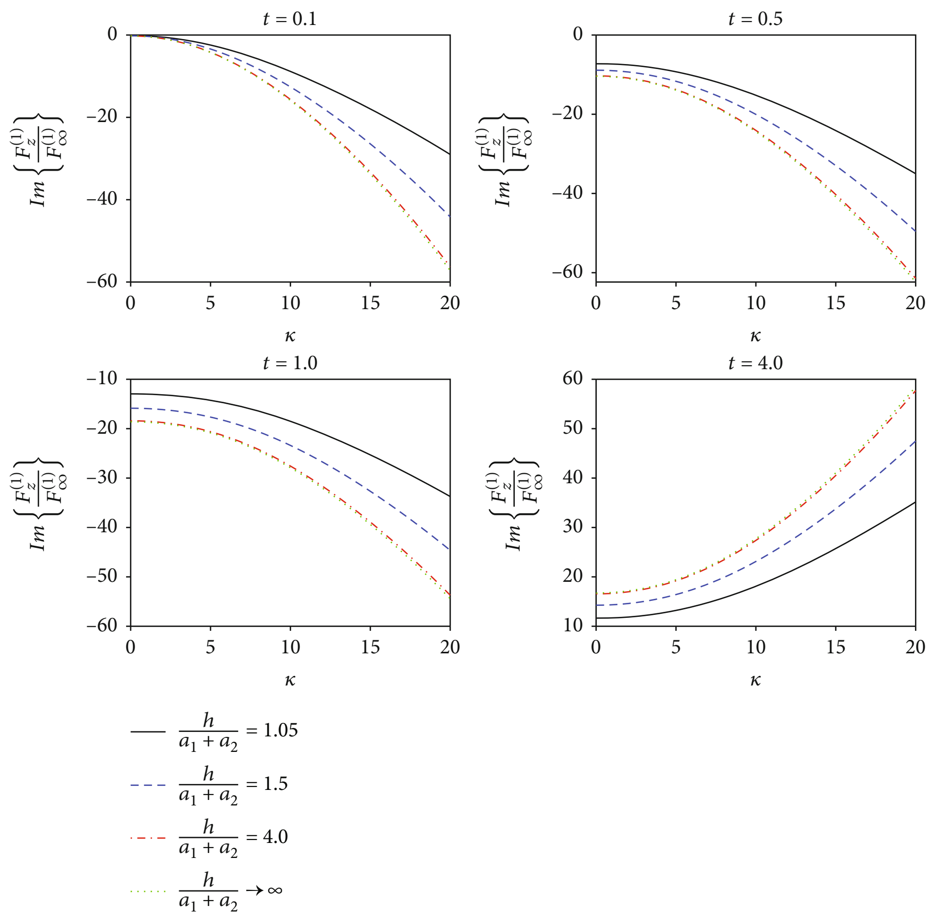

Figure 5: Time-dependent distribution of imaginary friction force on a sphere a_1 versus the frequency for different separation parameters with $a_2/a_1 = 4.0$, $U_2/U_1 = 1.0$, and $R_H = 10.0$.

[22], then we have

$$\psi' = \frac{\psi}{Ua^2}, \quad \vec{q}\,' = \frac{\vec{q}}{U}, \quad t' = \omega t, \quad \nabla^{2'} = a^2\nabla^2, \quad p' = \frac{ap}{\mu U}, \quad r' = \frac{r}{a}. \tag{8}$$

By using equation (8) into equation (2) and using equation (5), we have

$$\left(\frac{\omega a^2}{\mu}\right)\frac{\partial \vec{q}}{\partial t} = -\nabla p + \nabla^2\vec{q} - R_H^2\vec{q}. \tag{9}$$

In addition, we have

$$\left(R_m S_t \frac{\partial}{\partial t} + R_H^2\right)\vec{q} = -\nabla p + \nabla^2\vec{q}, \tag{10}$$

where $R_m = aU/\mu$ and $S_t = l\omega/U$ are the Reynolds and the Strouhal numbers, respectively, $(S_t >> 1, R_m << 1)$. From equation (9), the field equations with stream function terms are

$$\frac{\partial p}{\partial r} = -\frac{1}{r^2 \sin\theta}\frac{\partial}{\partial\theta}\left[R_H^2 - i\omega R_m S_t\right]\psi - \frac{1}{r^2\sin\theta}\frac{\partial}{\partial\theta}\left(E^2\psi\right), \tag{11}$$

$$\frac{1}{r}\frac{\partial p}{\partial\theta} = -\frac{1}{r\sin\theta}\frac{\partial}{\partial r}\left[R_H^2 - i\omega R_m S_t\right]\psi + \frac{1}{r\sin\theta}\frac{\partial}{\partial r}\left(E^2\psi\right). \tag{12}$$

Eliminating the pressure from equations (11) and (12), a fourth-order partial differential equation was obtained by using the stream function:

$$E^2\left(E^2 - \alpha^2\right)\psi = 0, \tag{13}$$

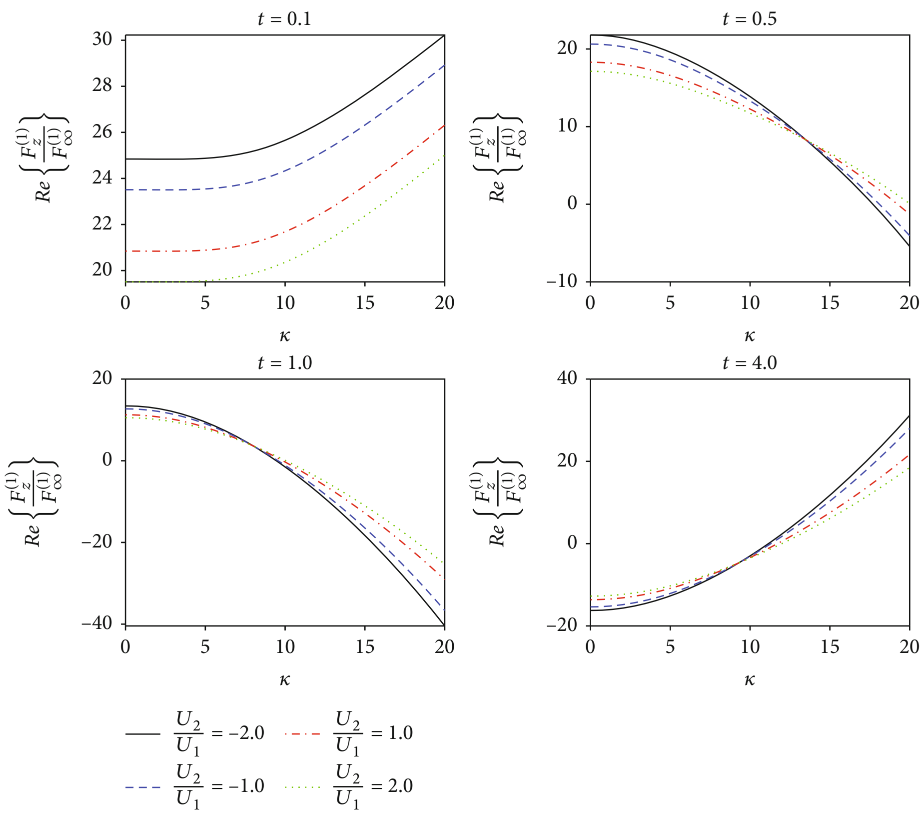

FIGURE 6: Time-dependent distribution of real friction force on a sphere a_1 versus the frequency for different separation parameters with $a_2/a_1 = 2.0$, $h/a_1 + a_2 = 1.5$, and $R_H = 10.0$.

where $\alpha = \sqrt{R_H^2 - i\kappa^2}$, $\kappa = \sqrt{a\omega/\nu^2}$ is the frequency parameter, $E^2 = (\partial^2/\partial r^2) + (1 - \xi^2/r^2)(\partial^2/\partial \xi^2)$ is the Stokesian operator, and $\xi = \cos\theta$. The consistent solution of (13) is as follows:

$$\psi(r,\theta) = \sum_{n=2}^{\infty}\left(A_n r^{-n+1} + B_n r^{1/2} K_{n-(1/2)}(\alpha r)\right)\mathfrak{I}_n(\xi), \quad (14)$$

where the Gegenbauer function is $\mathfrak{I}_n(.)$ of the first kind of order n and degree $-1/2$. The modified Bessel function is $K_n(.)$ of the second kind of order n. Thus, the components of velocity are calculated by

$$q_r(r,\theta) = -\sum_{n=2}^{\infty}\left[A_n r^{-n-1} + B_n r^{-3/2} K_{n-(1/2)}(\alpha r)\right] P_{n-1}(\xi), \quad (15)$$

$$q_\theta(r,\theta) = \sum_{n=2}^{\infty}\left[(1-n)A_n r^{-n-1} + B_n r^{-1/2}\left(nK_{n-(1/2)}(\alpha r) - \alpha r K_{n+(1/2)}(\alpha r)\right)\right]\frac{\mathfrak{I}_n(\xi)}{\sqrt{1-\xi^2}}, \quad (16)$$

where $P_n(.)$ is the polynomial of the Legendre of degree n. In the oscillating volume particle V, a nondimensional drag force operates by [15] and modified by [22]:

$$\frac{F_z}{\alpha^2} = \left(V + 4\pi \lim_{r\longrightarrow\infty}\frac{r\psi}{\sin^2\theta}\right)e^{-it}. \quad (17)$$

Additionally, equation (18) gives

$$\frac{F_z}{2\pi\mu\alpha^2} = \left(\frac{2}{3}a^3 U + A_2\right)e^{-it}. \quad (18)$$

A drag force into equation (18) can be normalized by acting upon a solid sphere a_1 swimming within an infinite viscous fluid region in the absence of another hard sphere without slippage, which is introduced by [15]:

$$F_\infty = -6\pi\mu a U. \quad (19)$$

4. The Problem Solution

The two rigid spheres of radii are $a_j, j = 1, 1$, and suppose that $a_2(a_2 > a_1)$. The influence by a magnetic field, axially oscillated inside an endless fluid flow of Stokes, suggests that the two hard spheres vibrate with respective amplitudes U_1 and U_2 going with the associating line of their centers which are isolated by a constant distance h. Then, the fluid flow stops at limitlessness. The system of spherical frameworks is utilized and formed over the focus of the two unbending spheres. In the meantime, the discoveries of this work are

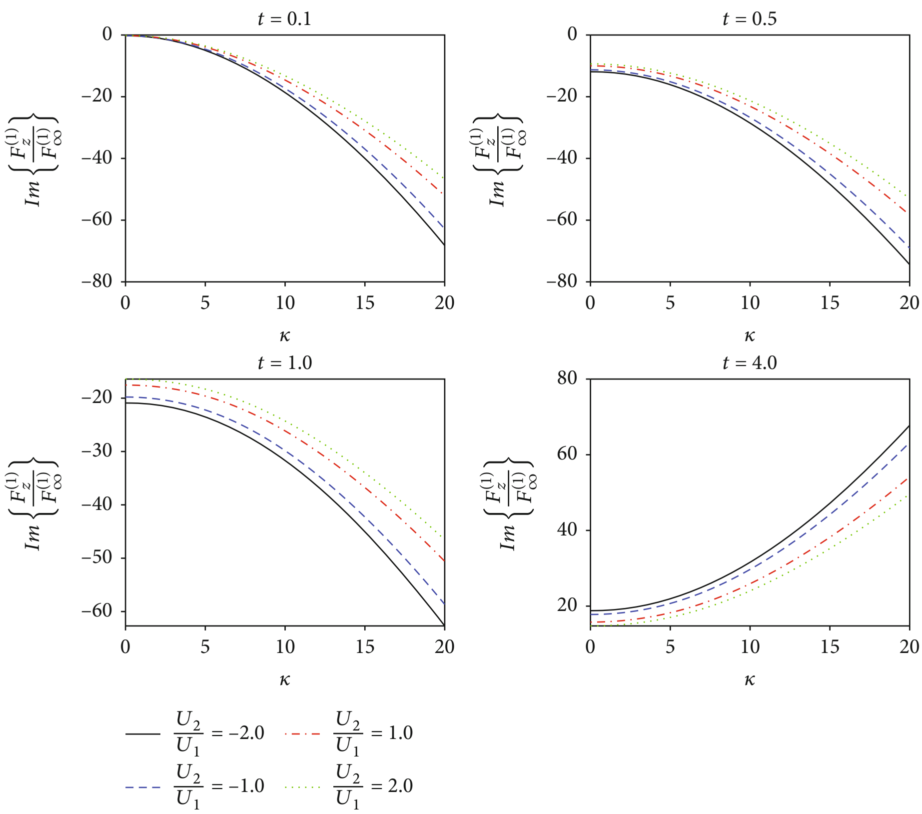

Figure 7: Time-dependent distribution of imaginary friction force on a sphere a_1 versus the frequency for different separation parameter with $a_2/a_1 = 2.0$, $h/a_1 + a_2 = 1.5$, and $R_H = 10.0$.

characterized in Figure 1. This connection between the two coordinates (r_1, θ_1) and (r_2, θ_2) is given by $r_2^2 = r_1^2 + h^2 + 2h\, r_1 \cos\theta_1, \theta_1)$ or $r_1^2 = r_2^2 + h^2 - 2hr_2 \cos\theta_2, \theta_1)$. Suppose the fluid velocities of the two solid spheres are

$$\vec{q}^{\,(j)}(r_j, \theta_j) = \left\langle q_r^{(j)}(r_j, \theta_j), q_\theta^{(j)}(r_j, \theta_j) \right\rangle. \tag{20}$$

4.1. Boundary Conditions. As a result of the components of the spheres' velocities approaching zero at an extended distance, the surfaces of solid spheres a_j, $j = 1, 1$ exhibit the following conditions:

(1) Impenetrability conditions:

$$q_r|_{r_j = a_j} = U_j \cos\theta_j, \quad j = 1, 2. \tag{21}$$

(2) Dynamical conditions:

$$q_\theta|_{r_j = a_j} = -U_j \sin\theta_j, \quad j = 1, 2. \tag{22}$$

By applying the superposition principle, we have

$$q_r(r_1, \theta_1 ; r_2, \theta_2) = q_r^{(1)}(r_1, \theta_1) + q_r^{(2)}(r_2, \theta_2), \tag{23}$$

$$q_\theta(r_1, \theta_1 ; r_2, \theta_2) = q_\theta^{(1)}(r_1, \theta_1) + q_\theta^{(2)}(r_2, \theta_2). \tag{24}$$

The function of the stream and the components of velocity are written in the following forms:

$$\begin{aligned}\psi(r, \theta) = {} & \sum_{n=2}^{\infty} \left[A_{1n}^{(1)} r_j^{-n+1} + B_{1n}^{(1)} r_1^{1/2} K_{n-(1/2)}(\alpha r_1) \right] \mathfrak{I}_n(\xi_1) \\ & + \sum_{n=2}^{\infty} \left[A_{2n}^{(2)} r_2^{-n+1} + B_{2n}^{(j)} r_2^{1/2} K_{n-(1/2)}(\alpha r_2) \right] \mathfrak{I}_n(\xi_2),\end{aligned} \tag{25}$$

$$\begin{aligned}q_r(r, \theta) = {} & -\sum_{n=2}^{\infty} \left(A_{1n}^{(1)} r_1^{-n-1} + B_{1n}^{(1)} r_1^{-3/2} K_{n-(1/2)}(\alpha r_1) \right) P_{n-1}(\xi_1) \\ & - \sum_{n=2}^{\infty} \left(A_{2n}^{(2)} r_2^{-n-1} + B_{2n}^{(2)} r_2^{-3/2} K_{n-(1/2)}(\alpha r_2) \right) P_{n-1}(\xi_2),\end{aligned} \tag{26}$$

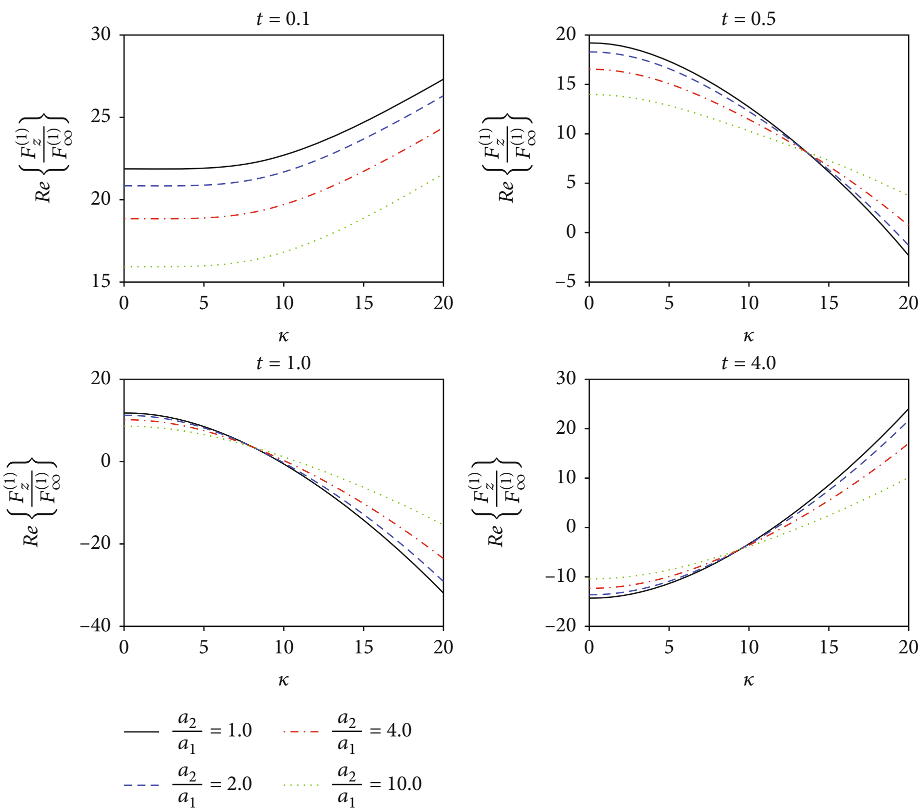

FIGURE 8: Time-dependent distribution of real friction force on a sphere a_1 versus the frequency for different separation parameters with $h/a_1 + a_2 = 1.5$, $U_2/U_1 = 1.0$, and $R_H = 10.0$.

$$\begin{aligned} q_\theta(r,\theta) = {} & \sum_{n=2}^{\infty}\Big[(1-n)A_1^{(1)} n r_1^{-n-1} + B_{1n}^{(1)} r_1^{-3/2}\Big(nK_{n-(1/2)}(\alpha r_1) \\ & - \alpha r_1 K_{n+(1/2)}(\alpha r_1)\Big)\Big]\frac{\mathfrak{I}_n(\xi_1)}{\sqrt{1-\xi_1^2}} \\ & + \sum_{n=2}^{\infty}\Big[(1-n)A_2^{(2)} n r_1^{-n-1} + B_{2n}^{(2)} r_2^{-3/2} \\ & \cdot \Big(nK_{n-(1/2)}(\alpha r_2) - \alpha r_2 K_{n+(1/2)}(\alpha r_2)\Big)\Big]\frac{\mathfrak{I}_n(\xi_2)}{\sqrt{1-\xi_2^2}}. \end{aligned} \tag{27}$$

Applying the boundary conditions from equations (21) and (22) into (24) and (25), we obtained the following four equations:

$$\begin{aligned} & \sum_{n=2}^{\infty}\Big[A_1 n a_1^{-n-1} + B_{1n} a_1^{-3/2} K_{n-(1/2)}(\alpha a_1)\Big] P_{n-1}(\xi_1) \\ & \quad + \sum_{n=2}^{\infty}\Big[A_2 n r_2^{-n-1} + B_{2n} r_2^{-3/2} K_{n-(1/2)}(\alpha r_2)\Big]_{r_1=a_1} P_{n-1}(\xi_2) = -U_1 \xi_1. \\ & \sum_{n=2}^{\infty}\big[A_{1n} r_1^{-n-1} + B_{1n} r_1^{-3/2} K_{n-1/2}(\alpha r_1)\big]_{r_2=a_2} P_{n-1}(\xi_1) \\ & \quad + \sum_{n=2}^{\infty}\Big[A_{2n} a_2^{-n-1} + B_{2n} a_2^{-3/2} K_{n-(1/2)}(\alpha r_2)\Big] P_{n-1}(\xi_2) = -U_2 \xi_2. \\ & \frac{\mathfrak{I}_n(\xi_1)}{\sqrt{1-\xi_1^2}} \sum_{n=2}^{\infty}\Big[-(n-1)A_{1n} a_1^{-n-1} + B_{1n} a_1^{-3/2}\Big(nK_{n-(1/2)}(\alpha a_1) \\ & \quad - \alpha a_1 K_{n+(1/2)}(\alpha a_1)\big] + \frac{\mathfrak{I}_n(\xi_2)}{\sqrt{1-\xi_2^2}} \sum_{n=2}^{\infty}\big[-(n-1)A_{2n} r_2^{-n-1} \\ & \quad + B_{2n} r_2^{-3/2}\Big(nK_{n-(1/2)}(\alpha r_2) - \alpha r_2 K_{n+(1/2)}(\alpha r_2)\Big]_{r_1=a_1} \\ & \quad = -U_1\sqrt{1-\xi_1^2}. \\ & \frac{\mathfrak{I}_n(\xi_1)}{\sqrt{1-\xi_1^2}} \sum_{n=2}^{\infty}\Big[-(n-1)A_{1n} r_1^{-n-1} + B_{1n} r_1^{-3/2}\Big(nK_{n-(1/2)}(\alpha r_1) \\ & \quad - \alpha r_1 K_{n+(1/2)}(\alpha r_1)\big]_{r_2=a_2} + \frac{\mathfrak{I}_n(\xi_2)}{\sqrt{1-\xi_2^2}} \sum_{n=2}^{\infty}\big[-(n-1)A_{2n} a_2^{-n-1} \\ & \quad + B_{2n} a_2^{-3/2}\Big(nK_{n-(1/2)}(\alpha a_2) - \alpha a_2 K_{n+(1/2)}(\alpha a_2)\Big] = -U_2\sqrt{1-\xi_2^2}. \end{aligned} \tag{28}$$

The procedure of the Gauss elimination is assumed to solve the above equations to get the constants $A_n^{(j)}$ and $B_n^{(j)}$, $j = 1, 2$. Then, by equations (18) and (19), we can obtain the following expression of the hydrodynamic nondimensional drag

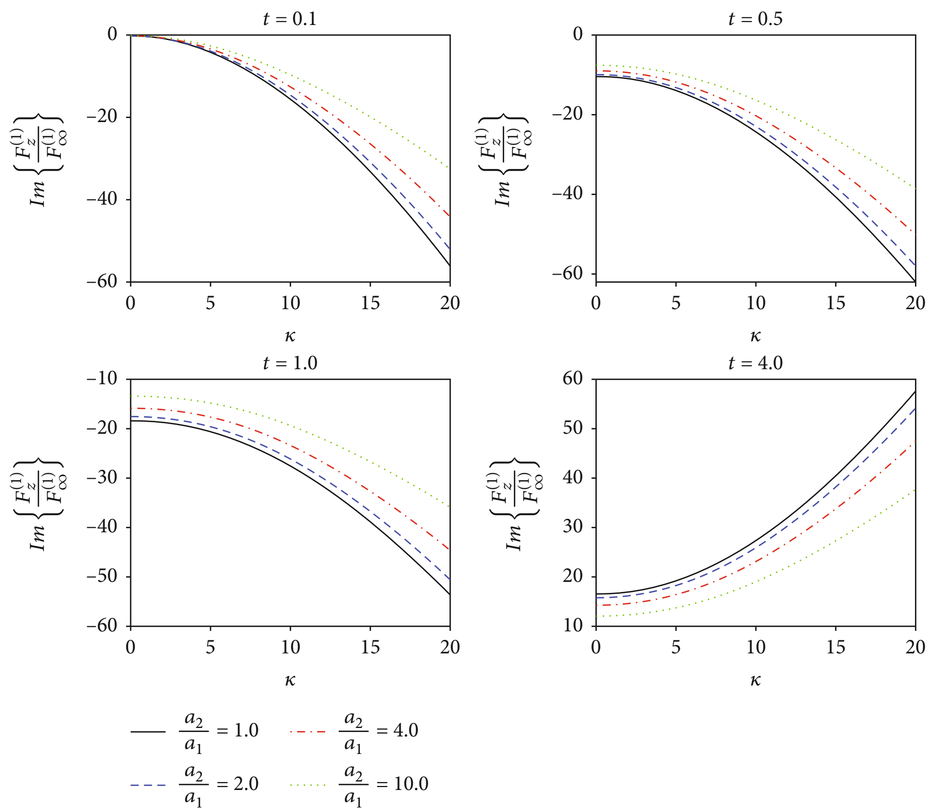

FIGURE 9: Time-dependent distribution of imaginary friction force on a sphere a_1 versus the frequency for different separation parameters with $h/a_1 + a_2 = 1.5$, $U_2/U_1 = 1.0$, and $R_H = 10.0$.

force coefficients on the particle a_1:

$$F_z^{(j)} = \frac{2}{3}\pi\mu\alpha^2\left(2a_j^3 U_j + 3A_{2n}^{(j)}\right)e^{-it} = \left(K_j + iK_j'\right)e^{-it}, \quad (29)$$

where

$$\begin{aligned} \text{Re}\left\{\frac{F_z^{(j)}}{F_\infty^{(j)}}\right\} &= K_j \cos t + K_j' \sin t, \\ \text{Im}\left\{\frac{F_z^{(j)}}{F_\infty^{(j)}}\right\} &= -K_j \sin t + K_j' \cos t, \end{aligned} \quad (30)$$

where K_j and K_j' are defined physically as in-phase and out-of phase forces of the oscillations, respectively.

5. Results and Discussions

In this paper, we describe the influence of the normal magnetic field upon two hard spheres that oscillate along their connecting lines and associate their centers. We show that the unsteady normalized drag force coefficients of the real part Re $\{F_z^{(1)}/F_\infty^{(1)}\}$ and the imaginary part Im $\{F_z^{(1)}/F_\infty^{(1)}\}$ act on the solid sphere a_1, respectively, shown in Figures 2–9 and Tables 1–3. Therefore, the two parts of forces are determined analytically and numerically for different relevant parameters as the number of the Hartmann R_H, the frequency κ, the parameter of separation $h/(a_2 + a_1)$, the velocity's ratio U_2/U_1, and the size ratio a_2/a_1. Physically, this means that the value and direction of the magnetic field oscillate with time at any point in the unbounded region. Furthermore, this means that the combined effect of the magnetic field and the oscillation on the particles will now experience a changing force, causing them to move with the wave. In fact, the real drag force coefficient is enhanced with the increase of the frequency and the magnetic field in the case of a small period of time and conversely for a large period of time. On the other side, the imaginary drag force coefficient disintegrates in the increase of the frequency parameters, but for the magnetic effects, it differs from a high or low level due to the period of time.

Figure 2 exposes an analysis of Re $\{F_z^{(1)}/F_\infty^{(1)}\}$ versus the frequency parameter for different values of time $t = 0.1, 0.5$ $, 1.0,$ and 4.0, and the number of the Hartmann number is $R_H = 0.0, 2.0, 6.0,$ and 10.0 that the two hard spheres oscillate with equal velocities and sizes with separation $h/a_2 + a_1 = 1.5$. Also, clearly, the nondimensional forces increment and diminish from least to greatest values at $t = 0.1$ and 4.0; with the growth of R_H, the forces reverse their effects, where at $t = 0.1$, they increase with the increase of R_H and converse at $t = 4.0$. Furthermore, this phenomenon has the lowest significance when the frequency becomes low and highest

Table 1: Time-dependent distribution of real drag force for different parameters with $t = 0.1$.

$h/a_1 + a_2$	κ	$U_2/U_1 = 1.0$ $R_H = 0.0$	$R_H = 1.0$	$R_H = 10.0$	$U_2/U_1 = -1.0$ $R_H = 0.0$	$R_H = 1.0$	$R_H = 10.0$
1.05	0.0	0.737106	1.956094	22.742968	1.604499	2.381086	21.742540
	2.0	2.127277	2.468029	22.678823	2.315930	2.617443	21.679880
	4.0	3.509225	3.719294	22.511454	3.196566	3.407236	21.514107
	6.0	4.633449	4.812597	22.312454	4.119232	4.295981	21.308851
	8.0	5.639012	5.802021	22.174961	4.984639	5.145009	21.148056
	10.0	6.545034	6.698222	22.160419	5.766347	5.917192	21.089533
1.5	0.0	0.855934	2.063856	21.764544	1.509353	2.139260	22.302687
	2.0	2.281406	2.577374	21.703287	2.134518	2.465844	22.238976
	4.0	3.397105	3.602867	21.543362	3.292780	3.504675	22.071772
	6.0	4.436660	4.609584	21.352989	4.343953	4.522521	21.869513
	8.0	5.398842	5.555285	21.221554	5.292153	5.454566	21.721756
	10.0	6.275108	6.421771	21.209362	6.147829	6.300527	21.688688
10.0	0.0	0.949419	2.100399	21.996012	1.045610	2.100730	22.005285
	2.0	2.216419	2.528693	21.933681	2.216784	2.529166	21.942924
	4.0	3.349177	3.557647	21.770565	3.349727	3.558286	21.779716
	6.0	4.393228	4.568616	21.574938	4.393896	4.569368	21.583952
	8.0	5.348567	5.507622	21.436214	5.349294	5.508429	21.445065
	10.0	6.215195	6.364499	21.414633	6.215923	6.365305	21.423302
∞	0.0	0.995011	2.100564	22.000648	0.995011	2.100564	22.000648
	2.0	2.216602	2.528929	21.938303	2.216602	2.528929	21.938303
	4.0	3.349452	3.557966	21.775141	3.349452	3.557966	21.775141
	6.0	4.393562	4.568992	21.579443	4.393562	4.568992	21.579443
	8.0	5.348931	5.508025	21.440639	5.348931	5.508025	21.440639
	10.0	6.215559	6.364902	21.418966	6.215559	6.364902	21.418966

significance when there is high hesitancy, but for the values $t = 0.5$ and 1.0, it rises with the growth of Hartmann numbers, and also, it has the most increased significance for low hesitancy and gradually goes to lowest values for the increased frequency. As expected, increasing R_H decreases flow amplitude. In this case, the magnetic field acts as a resistance to the flow.

Figure 3 shows an analysis of Im $\{F_z^{(1)}/F_\infty^{(1)}\}$ against the frequency for different values of time $t = 0.1, 0.5, 1.0,$ and 4.0 , and the Hartmann numbers $R_H = 0.0, 2.0, 6.0,$ and 10.0 move with equal velocities and equal size with $h/a_2 + a_1 = 1.5$. Hence, the dimensionless frictional force begins to improve and also diminishes from the greatest significance for low hesitancy to the lowest significance for the elevated hesitancy at $t = 0.5$ and 1.0, and hence, the drag force reverses the impact at $t = 4.0$ versus the frequency, while it reduces with the growth of R_H at $t = 0.5$ and 1.0 and improves at $t = 0.1$ and 4.0.

Figure 4 exhibits an analysis of Re $\{F_z^{(1)}/F_\infty^{(1)}\}$ versus the frequency for different separation distance $h/a_2 + a_1 = 1.05, 1.5, 4.0, \infty$ at times $t = 0.1, 0.5, 1.0,$ and 4.0 for $a_2/a_1 = 4.0$ action in the identical direction with equal speeds and $R_H = 10.0$. In addition, the nondimensional force increases with the expansion of the divergence space between the spheres from the lowest value at a lower frequency to the greatest value at an increased frequency. In addition, at $t = 0.5$, the real coefficient rises with the expansion of the separation distance and reverses its impacts at $(X, Y) = (13.2, 8.7058)$ with the same impact at $t = 1.0$ at this point $(X, Y) = (8, 3.63531)$, while at $t = 4.0$, it reduces and then grows with the expansion of the gap space at $(X, Y) = (9.2, -4.8439)$.

Figure 5 reveals the unsteady imaginary coefficient Im $\{F_z^{(1)}/F_\infty^{(1)}\}$ versus the frequency for different separation space $h/a_2 + a_1 = 1.05, 1.5, 4.0, \infty$ at times $t = 0.1, 0.5, 1.0,$ and 4.0 for $a_2/a_1 = 4.0$ with an equal size and $R_H = 10.0$. Moreover, the force coefficient reduces with the separation distance growth at $t = 0.1, 0.5,$ and 1.0 but reverses its direction at $t = 4.0$. While, for the beginning three time values, it started from high at the low frequency to low at the high frequency and finally reversing its direction.

Figure 6 presents an analysis of the real part Re $\{F_z^{(1)}/F_\infty^{(1)}\}$ against the frequency for various velocity ratios $U_2/U_1 = -2.0, -1.0, 1.0,$ and 2.0 at times $t = 0.1, 0.5, 1.0,$ and 4.0 for $a_2/a_1 = 2.0$, $h/a_2 + a_1 = 1.5$, and $R_H = 10.0$. Therefore, the nondimensional force diminishes with the

Table 2: Time-dependent distribution of imaginary drag force for different parameters with $t = 0.1$.

$h/a_1 + a_2$	κ	$U_2/U_1 = 1.0$			$U_2/U_1 = -1.0$		
		$R_H = 0.0$	$R_H = 1.0$	$R_H = 10.0$	$R_H = 0.0$	$R_H = 1.0$	$R_H = 10.0$
1.05	0.0	0.014958	0.196264	2.281908	0.062305	0.238905	2.181531
	2.0	2.313483	2.142515	2.942240	1.841162	1.749658	2.824662
	4.0	5.246850	5.172472	4.923199	4.725361	4.669257	4.754086
	6.0	9.063329	9.019673	8.210455	8.523103	8.485922	7.957600
	8.0	13.815021	13.785376	12.744536	13.202316	13.176731	12.383576
	10.0	19.482973	19.461624	18.416477	18.781002	18.762648	7.935371
1.5	0.0	0.104732	0.207076	2.183738	0.146120	0.214642	2.237733
	2.0	2.124735	1.982060	2.814270	2.058339	1.932504	2.892788
	4.0	4.914481	4.849117	4.705865	5.033382	4.965434	4.857947
	6.0	8.625447	8.584078	7.845160	8.853466	8.812407	8.119753
	8.0	13.196646	13.168102	12.176163	13.588350	13.560367	12.621916
	10.0	18.628876	18.608147	17.595196	19.237036	19.216887	18.260399
10.0	0.0	0.095628	0.210743	2.206963	0.104600	0.210776	2.207893
	2.0	2.090080	1.956012	2.848191	2.090725	1.956631	2.849446
	4.0	4.964515	4.898038	4.771873	4.966308	4.899822	4.774103
	6.0	8.723106	8.681906	7.964615	8.726628	8.685424	7.968464
	8.0	13.365860	13.337582	12.370331	13.371682	13.343403	12.376435
	10.0	18.892776	18.872316	17.885242	18.901468	18.881008	17.894215
∞	0.0	0.099845	0.210759	2.207428	0.099845	0.210759	2.207428
	2.0	2.090403	1.956322	2.848818	2.090403	1.956322	2.848818
	4.0	4.965411	4.898930	4.772988	4.965411	4.898930	4.772988
	6.0	8.724867	8.683664	7.966540	8.724867	8.683664	7.966540
	8.0	13.368771	13.340492	12.373383	13.368771	13.340492	12.373383
	10.0	18.897121	18.876661	17.889727	18.897121	18.876661	17.889727

improvement of the velocity ratios at $t = 0.1$ and begins from a minimum at the lower frequency to a maximum at the heightened frequency. In addition, the values of $t = 0.5$ and 1.0 decrease with the improvement of the ratio of the speeds and flip its impacts at the point $(X, Y) = (13.6, 8.18006)$ while it rises and then reduces from less to most at the time $t = 4.0$.

Figure 7 represents the normalized imaginary force Im $\{F_z^{(1)}/F_\infty^{(1)}\}$ versus the frequency for distinct speeds $U_2/U_1 = -2.0, -1.0, 1.0,$ and 2.0 and $t = 0.1, 0.5, 1.0,$ and 4.0 with $h/a_2 + a_1 = 1.5$ and $R_H = 10.0$. Due to this, the force improves as the velocity ratio grows at $t = 0.1, 0.5,$ and 1.0 and initiates from the most at the lower frequency to less at the heightened frequency. Therefore, at $t = 4.0$, it reduces with the expansion of the velocity's ratio from min to max.

Figure 8 displays an investigation of Re $\{F_z^{(1)}/F_\infty^{(1)}\}$ versus the frequency for distinct size ratio at times $t = 0.1$, $0.5, 1.0,$ and 4.0 for the two rigid spheres move in the identical path with $h/a_2 + a_1 = 1.5$ and $R_H = 10.0$. Also, the normalized force declines with the improvement of size ratio at $t = 0.1$, and for the time values $t = 0.5$ and 1.0, it reverses its effects at the point of reflection. However, it goes from a low value at a low frequency that is improving with respect to the size ratio and then goes to a high value at a high frequency where it is reducing as the ratio size improves at the point of inversion, $(X, Y) = (9.2, -4.75159)$ at the time value $t = 4.0$.

Figure 9 displays an analysis of the frictional force Im $\{F_z^{(1)}/F_\infty^{(1)}\}$ versus the frequency for different size ratios $a_2/a_1 = 1.0, 2.0, 4.0,$ and 10.0 for the two hard spheres moving in the same direction with equal size and $h/a_2 + a_1 = 1.5$ and $R_H = 10.0$. Moreover, the nondimensional drag force improves as the size ratio rises at $t = 0.1, 0.5,$ and 1.0, starting from the highest value to the lowest value at the high frequency, but at $t = 4.0$, the size ratio declined with increasing frequency, starting from the low frequency and then increasing to the heightened frequency. The two coefficients of drag forces are calculated numerically in Tables 1 and 2, but Table 3 represents the limiting case of the steady state and the comparison between this study and the case of the absence of a magnetic field in the work of Faltas and El-Sapa [7]. Finally, all the figures have the following behavior: the drag force coefficients are proportional to the frequency, and the Hartmann number distinguishes low and high frequency where they differ according to the time at high frequency.

Table 3: Comparison of the real and imaginary parts of drag force coefficients for spheres with the same size moving in the same direction for different relevant parameters at the steady state.

R_H	$\frac{a_1+a_2}{h}$	$\mathrm{Re}\left\{\frac{F_z^{(1)}}{F_\infty^{(1)}}\right\}$ $\kappa = 0.001$	$\kappa = 1.0$	$\kappa = 10.0$	$\mathrm{Im}\left\{\frac{F_z^{(1)}}{F_\infty^{(1)}}\right\}$ $\kappa = 0.001$	$\kappa = 1.0$	$\kappa = 10.0$
0.0	0.0	1.000707	1.707107	8.071068	-0.000707	-0.818218	-18.182178
	0.1	0.954897	1.706979	8.070275	-0.001278	-0.818067	-18.177900
	0.2	0.915261	1.706403	8.066340	-0.001173	-0.816729	-18.153742
	0.3	0.881792	1.712857	8.060099	-0.001082	-0.810913	-18.104197
	0.4	0.853876	1.731624	8.055985	-0.001004	-0.822532	-18.037106
	0.5	0.830904	1.735158	8.061214	-0.000937	-0.858508	-17.971771
	0.6	0.812182	1.709487	8.084454	-0.000880	-0.898281	-17.936876
	0.7	0.796809	1.661024	8.132718	-0.000830	-0.923711	-17.967096
	0.8	0.783453	1.601257	8.201556	-0.000785	-0.928828	-18.096043
	0.9	0.770626	1.538112	8.254853	-0.000744	-0.916600	-18.329855
1.0	0.0	2.111111	2.209795	8.217622	-0.000001	-0.566201	-18.146912
	0.1	2.110948	2.209604	8.216791	-0.000001	-0.566098	-18.142637
	0.2	2.110714	2.209111	8.212633	-0.000001	-0.565348	-18.118498
	0.3	2.111449	2.210530	8.205931	-0.000001	-0.563880	-18.068985
	0.4	2.111403	2.215577	8.201185	-0.000001	-0.566104	-18.001928
	0.5	2.106214	2.218520	8.205776	-0.000001	-0.576653	-17.936602
	0.6	2.092247	2.211147	8.228627	-0.000001	-0.593546	-17.901655
	0.7	2.067723	2.188815	8.277059	-0.000001	-0.610617	-17.931725
	0.8	2.031941	2.150701	8.346972	-0.000001	-0.622034	-18.060406
	0.9	1.986013	2.099322	8.402543	-0.000001	-0.625439	-18.294281
10.0	0.0	22.111111	22.111237	23.097952	0.000000	-0.161110	-15.662010
	0.1	22.106461	22.106586	23.093203	0.000000	-0.161070	-15.657987
	0.2	22.080599	22.080725	23.066809	0.000000	-0.160839	-15.635173
	0.3	22.028883	22.029007	23.014126	0.000000	-0.160363	-15.588047
	0.4	21.961988	21.962112	22.946213	0.000000	-0.159712	-15.523438
	0.5	21.903486	21.903612	22.887344	0.000000	-0.159063	-15.458811
	0.6	21.886805	21.886929	22.871883	0.000000	-0.158684	-15.420453
	0.7	21.949163	21.949287	22.938110	0.000000	-0.158900	-15.440438
	0.8	22.116991	22.117117	23.113535	0.000000	-0.160046	-15.551090
	0.9	22.385357	22.385485	23.389128	0.000000	-0.162350	-15.777214

6. Conclusion

The impact of the magnetic field on the interaction of two oscillating rigid spheres moving into an endless Stokes flow launching along the axis of symmetry is contemplated. We employed a semianalytical strategy and a collocation method to get the solution and hence calculate the nondimensional friction force coefficients. In the meantime, we determined the drag coefficients for different size proportions, speed proportions, separation distance, frequency parameters, and Hartmann numbers. Then again, it shows that in the case of low frequencies and the drag force, it starts at the most extreme and subsequently diminishes. Thus, it is more critical to notice the effects of the Hartman number that shows that the real part of the drag force diminishes by expanding the Hartmann number over a long time, though the imaginary part of the drag force increments by expanding the Hartmann number over a long time, and in the two cases, it begins from a base for low frequency and afterward comes to a maximum for high hesitation. Accordingly, the nondimensional drag force coefficients increment as the detachment distance develops at specific points in the frequency, and it reverses its impacts. Subsequently, it diminishes for the real force and increments for the coefficient of the imaginary drag force as the speed proportion rises. Faltas and El-Sapa [7] and Chen and Keh proposed great support and accuracy in the limiting cases. The future scope of this study may be in many fields of technology and in biomedicine, and magnetic oscillating particles have been used for years. In biomedicine, they are utilized in imaging, drug delivery, and magnetic hyperthermia (MH). Under the influence of alternating high-frequency magnetic fields, MH increases local temperatures in target cells by activating magnetic nanoparticles locally. The application of this study in the practical field may be presented as an experimental investigation of a sphere performing torsional oscillations in a Stokes flow. An experimental setup was developed that allowed the movement of the sphere to be remotely controlled by a magnetic field.

Data Availability

Data are available upon request to the corresponding author.

Conflicts of Interest

The authors declare that there are no conflicts of interest.

Authors' Contributions

Shreen El-Sapa contributed in the conceptualization, methodology, software provision, and data curation and wrote the original draft. Wedad Albalawi performed supervision, visualization, and investigation.

Acknowledgments

The authors express their gratitude to Princess Nourah bint Abdulrahman University Researchers Supporting Project number (PNURSP2023R157), Princess Nourah bint Abdulrahman University, Riyadh, Saudi Arabia.

References

[1] S. S. Tabakova and Z. D. Zapryanov, "On the hydrodynamic interaction of two spheres oscillating in a viscous fluid.? I. Axisymmetrical case," *ZAMP*, vol. 33, no. 3, pp. 344–357, 1982.

[2] L. Schouveiler, A. Brydon, T. Leweke, and M. C. Thompson, "Interactions of the wakes of two spheres placed side by side," *European Journal of Mechanics - B/Fluids*, vol. 23, no. 1, pp. 137–145, 2004.

[3] D. Klotsa, M. R. Swift, R. Bowley, and P. King, "Interaction of spheres in oscillatory fluid flows," *Physical Review E*, vol. 76, no. 5, article 056314, 2007.

[4] F. Otto, E. K. Riegler, and G. A. Voth, "Measurements of the steady streaming flow around oscillating spheres using three dimensional particle tracking velocimetry," *Physics of Fluids*, vol. 20, no. 9, article 093304, 2008.

[5] F. Box, K. Singh, and T. Mullin, "The interaction between rotationally oscillating spheres and solid boundaries in a stokes flow," *Journal of Fluid Mechanics*, vol. 849, pp. 834–859, 2018.

[6] T. J. van Overveld, M. Shajahan, W.-P. Breugem, H. J. Clercx, and M. Duran-Matute, "Numerical study of a pair of spheres in an oscillating box filled with viscous fluid," *Physical Review Fluids*, vol. 7, no. 1, article 014308, 2022.

[7] M. S. Faltas and S. El-Sapa, "Rectilinear oscillations of two spherical particles embedded in an unbounded viscous fluid," *Microsystem Technologies*, vol. 25, no. 1, pp. 39–49, 2019.

[8] C. Plumpton and V. C. A. Ferraro, "On toroidal magnetic fields in the sun and stars," *Astrophysical Journal*, vol. 121, p. 168, 1955.

[9] K. Stewartson, "On asymptotic expansions in the theory of boundary layers," *Journal of Mathematics and Physics*, vol. 36, pp. 171–191, 1957.

[10] M. P. Singh, "Drag of a sphere oscillating in a conducting viscous medium," *The Physics of Fluids*, vol. 9, pp. 797–805, 1965.

[11] H. M. Barakat, "Magnetohydrodynamic (MHD) stability of oscillating fluid cylinder with magnetic field," *Journal of Applied & Computational Mathematics*, vol. 4, p. 271, 2015.

[12] R. Wentzell, "Torsional oscillations of a fluid sphere with a rigid boundary in a uniform magnetic field," *Journal of Fluid Mechanics*, vol. 24, no. 2, pp. 275–284, 1966.

[13] A. M. Morad, S. M. A. Maize, A. A. Nowaya, and Y. S. Rammah, "Stability analysis of magnetohydrodynamics waves in compressible turbulent plasma," *Journal of Nanofluids*, vol. 9, no. 3, pp. 196–202, 2020.

[14] A. M. Morad, S. M. A. Maize, A. A. Nowaya, and Y. S. Rammah, "A new derivation of exact solutions for incompressible magnetohydrodynamic plasma turbulence," *Journal of Nanofluids*, vol. 10, no. 1, pp. 98–105, 2021.

[15] C. J. Lawrence and S. Weinbaum, "The force on an axisymmetric body in linearized, time-dependent motion: a new memory term," *Journal of Fluid Mechanics*, vol. 171, pp. 209–218, 1986.

[16] M. M. Bhatti and I. Sara, "Scientific breakdown of a ferromagnetic nanofluid in hemodynamics: enhanced therapeutic approach," *Mathematical Modelling of Natural Phenomena*, vol. 17, no. 44, p. 44, 2022.

[17] X. Cai, G. H. Su, and S. Qiu, "Upwinding meshfree point collocation method for steady MHD flow with arbitrary orientation of applied magnetic field at high Hartmann numbers," *Computers and Fluids*, vol. 44, no. 1, pp. 153–161, 2011.

[18] S. Rashidi, J. A. Esfahani, and M. Maskaniyan, "Applications of magnetohydrodynamics in biological systems-a review on the numerical studies," *Journal of Magnetism and Magnetic Materials*, vol. 439, pp. 358–372, 2017.

[19] M. Dhivya, P. Loganathan, and K. Vajravelu, "Chemically reacting viscous fluid flow on a permeable cylinder susceptible to oscillations," *International Communications in Heat and Mass Transfer*, vol. 126, article 105477, 2021.

[20] Y. Li, A. Anyuang Deng, L. Zhang, B. Yang, and E. Wang, "A new type of magnetic field arrangement to suppress meniscus fluctuation in slab casting: numerical simulation and experiment," *Journal of Materials Processing Technology*, vol. 298, article 117278, 2021.

[21] S. El-Sapa, "Interaction between a non-concentric rigid sphere immersed in a micropolar fluid and a spherical envelope with slip regime," *Journal of Molecular Liquids*, vol. 351, article 118611, 2022.

[22] S. El-Sapa and M. S. Faltas, "Mobilities of two spherical particles immersed in a magneto-micropolar fluid," *Physics of Fluids*, vol. 34, no. 1, article 013104, 2022.

[23] P. K. Yadav, S. Deao, and A. N. Filippov, "Effect of magnetic field on the hydrodynamic permeability of a membrane built up by porous spherical particles," *Colloid Journal*, vol. 79, no. 1, pp. 160–171, 2017.

[24] S. El-Sapa and W. Alhejaili, "On the hydrodynamic interaction of two coaxial spheres oscillating in a viscous fluid with a slip regime," *Journal of Applied Mathematics and Mechanics*, vol. 103, no. 3, 2023.

[25] M. Faizan, F. Ali, K. Loganathan, A. Zaib, C. A. Reddy, and S. I. Abdelsalam, "Entropy analysis of Sutterby nanofluid flow over a Riga sheet with gyrotactic microorganisms and Cattaneo–Christov double diffusion," *Mathematics*, vol. 10, no. 17, p. 3157, 2022.